Investigation of Solid Surfaces Modified by Langmuir−Blodgett Monolayers Using Sum-Frequency Vibrational Spectroscopy and X-ray Photoelectron Spectroscopy

Tamás Keszthelyi,*,[†] Zoltán Pászti,[†] Tímea Rigó,[†] Orsolya Hakkel,[†] Judit Telegdi,[†] and László Guczi[†,‡]

Institute of Surface Chemistry and Catalysis, Chemical Research Centre, P.O. Box 17, H-1525 Budapest, Hungary, and Institute of Isotopes, Chemical Research Centre, P.O. Box 77, H-1525 Budapest, Hungary

Langmuir−Blodgett (LB) monomolecular layers of alkylhydroxamic acids and alkylphosphonic acids on copper and iron substrates have been studied by X-ray photoelectron spectroscopy (XPS) and sum-frequency vibrational spectroscopy. According to the XPS results, the structures of the hydroxamic acid and phosphonic acid Langmuir−Blodgett films are very similar: the thickness of the layer of the hydrocarbon tails is typically 1.9−2.1 nm, while the layer of headgroups is about 0.3−0.35 nm thick. The tilt angle of the carbon chains is estimated to be 20−30° with respect to the sample surface normal, and the molecules are connected to the substrate via their headgroups. Analysis of the P 2p and N 1s lines indicates the presence of deprotonated headgroups. The substrate Cu 2p line includes a component which can be assigned to Cu^{2+} ions in a thin $Cu(OH)_2$ layer. The deposition of LB layers led to significant decrease of the hydroxide-related signal, which indicates that binding of the headgroups to the surface is accompanied by the elimination of water molecules. The sum-frequency spectra also clearly indicate that well-ordered monolayers can be formed by the Langmuir−Blodgett technique. Since the nonresonant background from the metal substrates renders the analysis of the spectra more difficult, model system samples on glass were prepared. It was found that the alkyl chains of the adsorbed acids predominantly adopt the all-trans conformation and form an ordered structure. Upper limits for the mean tilt angle of the terminal methyl groups are ∼10−20°.

Introduction

Through the application of mono- and multimolecular layers, the planned and problem-oriented modification of surfaces can be achieved. Self-assembly of molecular layers from solution[1] and the Langmuir−Blodgett (LB) technique[2,3] are often used for the preparation of surface nanolayers.[4] Both preparation methods result in mono- and/or multimolecular layer covered solid surfaces. Molecular self-assembly is a spontaneous process in which the layer is formed by amphiphilic molecules that adsorb on the active sites of solids, while the LB technique, the transfer of ordered monolayers of amphiphilic molecules from the liquid/air interface to a solid substrate, is a directed and precisely controllable procedure. The LB technique allows the deposition of one or more monolayers, resulting in a tailored surface with well-defined layer thickness and structure. The formation of stable, packed, continuous molecular layers makes these techniques suitable candidates for corrosion protection applications, since with well-chosen compounds metal surfaces can be coated with stable protecting films. This type of research has considerable environmental importance as well, since it can lead to the replacement of traditional techniques and thereby decrease the synthetic chemical burden on the environment.

Initially silver and copper were functionalized by different amphiphiles, mainly by thiols and mercapto derivatives.[5−12] Later the modification of other metals, like iron, nickel, and titanium, by alkyl carboxylic and phosphonic acids,[13−18] by quaternary ammonium and silane derivatives,[19−22] and by alkyl thiosulfate[23] resulted in more corrosion-resistant surfaces due to the blocking effect of the amphiphiles on the active sites of the metals. The corrosion inhibition efficiency of these nanolayers depends on the layer thickness, on the headgroup, and on the hydrophobic chain in the amphiphiles.

The effectiveness of LB multimolecular films in corrosion inhibition depends mainly on the bulkiness of the hydrophobic part of the amphiphiles and on the number of layers. When the same amphiphilic molecules form a self-assembled molecular layer on solids, mainly the headgroups influence the layer formation. The protection efficiency of the nanolayers is also influenced by the compactness of the layers and especially by the ordering of the molecules in the films.

We have recently studied the behavior of mono- and multimolecular layers of alkylhydroxamic acids and alkylphosphonic acids on iron and copper surfaces. On these metal surfaces the self-assembly of hydroxamic acids is much faster than that of phosphonic acids.[24−27] The inhibition efficiency of the self-assembled layer was equivalent with five LB monolayers in agreement with literature data.[28] The monolayers can inhibit not only the corrosion but also other processes such as the adhesion of corrosion relevant microorganisms that can deteriorate metals.[29] The nanolayers of the hydroxamic acids control microbial attachment more effectively than those of the phosphonic acids, which is very important from the point of microbiologically influenced corrosion because the planktonic population is less dangerous than those embedded into biofilms.

* To whom correspondence should be addressed. E-mail: ktamas@ chemres.hu.
† Institute of Surface Chemistry and Catalysis.
‡ Institute of Isotopes.

8702 *J. Phys. Chem. B, Vol. 110, No. 17, 2006*

Keszthelyi et al.

CHART 1: Structural Formulas of Octadecanoylhydroxamic Acid (C18N) and Octadecylphosphonic Acid (C18P)
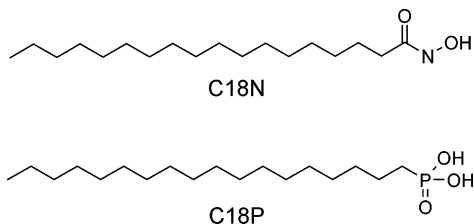
Here we employ infrared-visible sum-frequency generation vibrational spectroscopy and X-ray photoelectron spectroscopy (XPS) for the investigation of these monomolecular layer modified surfaces. Sum-frequency vibrational spectroscopy is a second-order nonlinear optical technique that, due to its inherent surface specificity, has been widely used for the investigation of interfacial phenomena.[30-33] The applicability and usefulness of sum-frequency vibrational spectroscopy for investigating the properties of LB layers[34-36] and self-assembled monolayers[37-49] on various surfaces have been demonstrated by several research groups.

In the present work we focus our investigations to monomolecular layers of long-chain alkylhydroxamic acids and alkylphosphonic acids, namely, octadecanoylhydroxamic acid (C18N) and octadecylphosphonic acid (C18P). Their structural formulas are shown in Chart 1. LB monomolecular layers of C18N and C18P were prepared on glass, iron, and copper substrates. Sum-frequency spectroscopy was used to derive information concerning the conformation and orientation of the alkyl chains in the Langmuir-Blodgett monolayers. In favorable cases it is possible to extract information about the orientation of methyl groups from the sum-frequency spectra, and the relevant formulas are given in the literature for the case of a methyl group of C_{3v} symmetry.[50] Our spectra clearly indicate that in the LB monolayers the symmetry of the terminal methyl groups is reduced to C_s, thus we had to work out the formulas applicable to this point group. The pertinent elements of the hyperpolarizability tensor were obtained from density functional theory (DFT) calculations. Quantitative XPS analysis gives further details about the structure of the LB layers. In addition, XPS is used to get a deeper insight into the bond formation processes between the headgroups and the metal substrates.

Experimental Details

Sample Preparation. Octadecanoylhydroxamic acid was prepared in our laboratory from the corresponding acyl chloride.[51] Octadecylphosphonic acid was synthesized according to the Michaelis-Arbusov method.[52] Ultrapure water used as the subphase for the LB film preparation was produced by a Millipore system (18.2 MΩ cm resistivity). The spreading solvent was analytical grade chloroform (Chemolab Ltd., Hungary). The glass, copper (high purity 99.99% polycrystalline Cu), and iron (armco 99.8% Fe) substrates were 10 mm by 14 mm in size.

The glass substrates were cleaned in chromic acid, and soaked in piranha solution (H_2O_2/concentrated H_2SO_4 = 1:2) before monolayer preparation. They were washed several times with copious amounts of deionized water and finally sonicated in ethanol for 15 min. Chromic acid, hydrogen peroxide, sulfuric acid, and ethanol were purchased from Reanal Ltd., Budapest, Hungary.

The metal substrates were polished first with SiC paper and then with diamond paste to a finish of 0.25 μm. Following each intermediate polishing step the substrates were sonicated in ethanol, while acetone was used as the cleaning solvent after the final polishing step.

LB films were prepared using an LB trough (NIMA Technology Ltd., 611D). Films were spread from chloroform solution onto the aqueous subphase (pH 5.6; 23 °C), and transferred to the solid substrates at a speed of 10 mm/min.

X-ray Photoelectron Spectroscopy. X-ray photoelectron spectroscopy measurements were carried out using an electron spectrometer manufactured by OMICRON Nanotechnology GmbH (Germany) with an EA125 energy analyzer. The photoelectrons were excited by Al Kα (1486.6 eV) radiation. Spectra were recorded in the Constant Analyser Energy mode: for survey spectra 50 eV pass energy was used, while detailed scans of LB film material and substrate related peaks were measured at 20 eV pass energy, with resolution better than 1 eV. The pressure during the measurements was lower than 5×10^{-10} mbar.

Most spectra presented here were recorded at normal emission (0° tilt angle between the sample surface normal and the direction to the analyzer). For quantitative purposes, angle-resolved XPS measurements were also carried out at different detection angles (between 0° and 55° with respect to the surface normal). LB films deposited on iron turned out to be relatively insensitive to radiation damage, while—despite the low X-ray power (150 W) and high X-ray source-to-sample distance (2 cm)—degradation of the layers on copper was quite fast, hindering the extensive use of the angle-resolved data for structural analysis.

Detailed spectra were processed by the Spectra Presenter software provided by OMICRON GmbH. After a Shirley or linear background was removed, spectra were fitted with Gaussian-Lorentzian sum peaks. Binding energies were referenced to the aliphatic component of the C 1s spectrum (285.0 eV binding energy), and the calibration was checked against substrate related features, such as the Fermi edge of metallic iron (0 eV binding energy). The binding energy scale was found to be consistent within 0.1-0.2 eV, indicating also that negligible charging occurred during the measurements.

Sum-Frequency Spectroscopy. Sum-frequency spectra were collected by an EKSPLA[53] (Vilnius, Lithuania) sum-frequency spectrometer. The visible beam (532 nm) is generated by doubling the fundamental output of a Nd:YAG laser (1064 nm wavelength, 20 ps pulse width, 20 Hz repetition rate). The tunable IR beam is obtained from an optical parametric generation/difference frequency generation system, pumped by the third harmonic and the fundamental of the Nd:YAG laser. The IR and visible beams are temporally and spatially overlapped on the sample surface with incident angles of 55° and 60°, respectively. To avoid damage of the metallic substrates, beam energies at the sample did not exceed 70 μJ, while in the case of the glass substrates, beam energies were kept below 200 μJ. Sum frequency light is collected in the reflected direction through a holographic notch filter and monochromator, and detected by a photomultiplier tube. Spectral resolution is determined by the <6 cm^{-1} line width of the IR pulse. Spectra presented were measured using the ssp (s-polarized sum-frequency, s-polarized visible, and p-polarized IR radiation), sps, and ppp polarization combinations. Spectra were collected in the 2800-3000 cm^{-1} spectral region using 3 cm^{-1} increments and 100 laser pulses at each step. Five to 10 such spectra were collected and averaged.

Calculation of the Molecular Hyperpolarizabilities. The dipole derivatives and polarizability derivatives with respect to Cartesian coordinates of the C18N and C18P molecules were obtained from DFT calculations at the optimized geometries. Geometry optimizations were carried out with the constraint of C_s symmetry. DFT calculations were performed with Gaussian98,[54] using the B3-LYP pair of exchange-correlation functionals and the 6-31G* basis set. The Cartesian dipole and polarizability derivatives were transformed into derivatives with respect to normal coordinates using the MOLVIB program of Sundius.[55]

Spectroscopy Background

Quantitative XPS Analysis. XPS is an especially useful tool for structural evaluation of samples consisting of thin layers, such as LB films on solid substrates. According to the theory of XPS, the intensity of a given peak depends on the distribution of the corresponding element in the direction perpendicular to the sample normal

$$I(E) = \Phi A \sigma(E, h\nu) L(\gamma) T(E) \int N(z) e^{-z/\lambda^m(E)\cos\vartheta} \, dz \quad (1)$$

where $N(z)$ (atom/cm³) is the depth-dependent concentration distribution of the element emitting photoelectrons of kinetic energy E, Φ is the flux of the exciting X-ray radiation, A is the analyzed surface area of the sample, $\sigma(E, h\nu)$ is the photoionization cross section of the corresponding core level at the exciting photon energy, $h\nu$, $L(\gamma)$ is a parameter characteristic for the angular distribution of photoelectrons, which depends on the angle between the X-ray beam and the direction of the analyzer, $T(E)$ is the transmission function of the analyzer at kinetic energy E, $\lambda^m(E)$ is the inelastic mean free path of the excited electron in the matrix m, and ϑ is the angle of the detection of the electrons with respect to the sample surface normal.[56]

Quantitative analysis of layered structures is usually carried out by establishing a mathematical model of the sample with parameters such as the thickness and composition of each individual layer. Then the relative intensities of the constituents of the sample are calculated using eq 1, and the parameters of the model are adjusted until the fit between the calculated and measured relative intensities is satisfactory. Reliability of the analysis can be significantly improved if intensity data sets measured at different detection angles are available.

In this work the XPS MultiQuant software[57] was used for the intensity calculations. Beyond evaluation of eq 1, the software incorporates tables of photoionization cross sections or sensitivity factors, calculates the appropriate inelastic mean free paths in each layer, and takes care of corrections for the analyzer transmission or the angular distribution of the excited electrons. The cross sections used here were based on the data set by Wagner et al.,[58] while the inelastic mean free path values were calculated by the method of Tanuma, Powell, and Penn.[59,60]

Sum-Frequency Spectroscopy. According to the basic theory of sum-frequency generation[30,61] the sum-frequency intensity in the reflected direction is proportional to the square modulus of the nonlinear susceptibility, $\chi^{(2)}$. For an azimuthally isotropic interface, only the χ_{yyz} component of the second-order susceptibility tensor contributes to the effective nonlinear susceptibility under the ssp polarization combination and only the χ_{yzy} component under the sps polarization combination. Under the ppp combination the effective susceptibility contains contributions from the χ_{xxz}, χ_{xzx}, χ_{zxx}, and χ_{zzz} tensor components.

The susceptibility has a resonant and a nonresonant contribution

$$\chi^{(2)} = \chi^{(2)}_{NR} + \chi^{(2)}_{R} = \chi^{(2)}_{NR} + \sum_m \frac{\chi^{(2)}_m}{\omega_2 - \omega_m + i\Gamma_m} \quad (2)$$

where $\chi^{(2)}_m$ is the resonant amplitude, ω_2 the frequency of the IR beam, and ω_m is a characteristic molecular vibrational frequency of the interface. From eq 2 it is seen that the sum-frequency intensity is therefore resonantly enhanced when the IR frequency matches the frequency of a molecular vibration. Thus by scanning the frequency of the infrared laser beam the vibrational spectrum of the interfacial molecules can be recorded. Accordingly, the spectra can be fit to the general formula

$$S(\omega_2) = \left| A_{NR} e^{i\varphi_{NR}} + \sum_m \frac{A_m e^{i\varphi_m}}{\omega_2 - \omega_m + i\Gamma_m} \right|^2 \quad (3)$$

In case of the ssp, sps, and pss polarization combinations, there is only contribution from a single susceptibility tensor component, and it can be shown[62] that the φ_m phases corresponding to the individual molecular vibrations are equal. In the case of the ppp polarization combination, there is contribution from four tensor components, and the φ_m phases of the individual vibrations can be different from each other.[62]

The susceptibility, in turn, is related to the molecular hyperpolarizability, $\alpha^{(2)}$ through the relation

$$\chi^{(2)}_{ijk} = N_s \sum_{a,b,c} \langle \Omega_{abc,ijk} \rangle \alpha^{(2)}_{abc} \quad (4)$$

where N_s is the number density of the surface molecules, and the transformation coefficients $\langle \Omega_{abc,ijk} \rangle$ are expressed in terms of the Euler angles defining the mutual orientation of the molecular (a,b,c) and laboratory (i,j,k) coordinate systems. The angular brackets denote an average over the molecular orientational distribution. If we make the usual assumption that the methyl group has C_{3v} symmetry, there are only two independent nonvanishing components of the hyperpolarizability for the symmetric stretch mode, $\alpha_{aac} = \alpha_{bbc}$, and α_{ccc}, and the above equation reduces to

$$\chi_{yyz,s} = \frac{1}{2} N_s \alpha_{ccc}[\langle \cos\theta \rangle(1 + r) - \langle \cos^3\theta \rangle(1 - r)]$$

$$\chi_{yzy,s} = \frac{1}{2} N_s \alpha_{ccc}[\langle \cos\theta \rangle - \langle \cos^3\theta \rangle](1 - r) \quad (5)$$

where $r = \alpha_{aac}/\alpha_{ccc}$ and θ is the polar angle (tilt) between the molecular c axis (the C_3 axis of the methyl group) and the laboratory z axis (the surface normal).

In the case of the antisymmetric methyl stretch mode

$$\chi_{yyz,as} = -\frac{1}{2} N_s \alpha_{aca}[\langle \cos\theta \rangle - \langle \cos^3\theta \rangle]$$

$$\chi_{yzy,as} = \frac{1}{2} N_s \alpha_{aca}\langle \cos^3\theta \rangle \quad (6)$$

In the literature certain ratios of the susceptibility tensor components, or alternatively of the corresponding peak amplitudes, are often used to extract information on the orientation distribution of methyl groups from the sum-frequency spectra.[63] The $\chi_{yzy,as}/\chi_{yyz,as}$ ratio,[64-67]—corresponding to the $A_{sps,r}/A_{ssp,r}$

ratio of the antisymmetric methyl stretch amplitudes from the sps and ssp spectra—and the $\chi_{yyz,s}/\chi_{yyz,as}$ ratio[66,68]—corresponding to the $A_{ssp,r^+}/A_{ssp,r^-}$ methyl symmetric stretch to methyl antisymmetric stretch amplitude ratio of the ssp spectra—have been successfully applied to the orientational analysis of methyl groups.

Sum-frequency spectra are also very sensitive to the conformation of the alkyl chains, as in the case of an all-trans chain, the methylene modes (d^+, d^-, and d^+_{FR}) are SF inactive due to their local centrosymmetry. The presence of the methylene modes in sum-frequency spectra is generally taken as an indication of gauche defects in the alkyl chains, and in fact the intensity ratio of the symmetric methylene and methyl modes, I_{d^+}/I_{r^+}, is often taken as a measure of the conformational order of alkyl chains.[63,69]

The elements of the molecular hyperpolarizability for a given vibrational normal mode, Q_m, can be calculated from the derivatives of the dipole moment ($\partial\mu/\partial Q_m$) and polarizability ($\partial\alpha/\partial Q_m$) with respect to the normal coordinate, as[70-72]

$$\alpha^{(2)}_{abc,m} = -\frac{1}{2\epsilon_0\omega_m}\left(\frac{\partial\alpha_{ab}}{\partial Q_m}\right)\left(\frac{\partial\mu_c}{\partial Q_m}\right) \quad (7)$$

Photoelectron Spectroscopy Results

Untreated Substrates. XPS spectra of several iron and copper reference samples were measured before depositing the LB films. Apart from the metal-related peaks, both kinds of samples exhibited strong oxygen and significant carbon signals, indicating that the initial surfaces are covered by metal oxide as well as a hydrocarbon contamination layer. There were no obvious changes in the XPS spectra after dipping the samples in the Langmuir trough filled with clean water; thus we can suppose that interaction with water does not influence the surface chemical properties of the substrates during LB film preparation.

Analysis of the binding energies of the substrate-related metal and oxygen peaks gives important information about the chemical state of the surfaces prior to LB film deposition. As far as the copper substrates are concerned, the main component of the Cu $2p_{3/2}$ peak was found at 932.7 eV binding energy (see Figure 4). The peak at 916.6 eV kinetic energy in the Cu LVV Auger spectrum revealed that the Cu $2p_{3/2}$ signal arises mostly from the Cu^+ ions of the oxide layer, which, accordingly, consists of mainly the Cu_2O phase.[73] A shoulder at 918.2−918.3 eV in the Cu LVV spectrum, which can be assigned to metallic copper, indicates that the oxide layer is not thicker than a few nanometers, thus electrons from the underlying metal can escape through it. In addition, a minor Cu $2p_{3/2}$ component at 934.3−934.6 eV binding energy, along with a satellite structure at around 943 eV, demonstrates the presence of Cu^{2+} ions.

Careful investigations[74,75] showed that the uppermost atomic layers of copper oxide films grown at low temperature contain Cu^{2+} ions in the form of CuO or $Cu(OH)_2$, while the bulk of the film consists of Cu^+ species. The binding energy of the Cu^{2+} states found on our untreated substrates (see Figure 4 below) suggests that the copper ions are connected to hydroxyl groups rather than to oxygen,[73,74] thus indicating the formation of a surface $Cu(OH)_2$ layer on the top of the copper oxide film. The O 1s spectrum, shown in Figure 1, is in agreement with the assignment of the copper-related signals: the main peak at 530.5−530.7 eV is due to oxygen atoms of the Cu_2O phase, while a broad feature around 531.6−532.0 eV contains contributions from the hydroxyl groups as well as the hydrocarbon contamination. This hydroxylated layer seems to play an important role in the bonding of the C18P and C18N molecules,
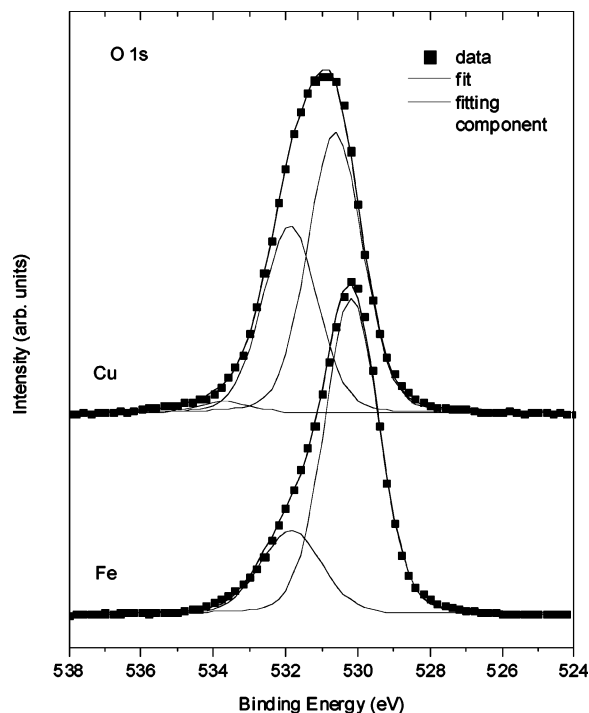

Figure 1. O 1s spectra of the untreated copper and iron substrates. The spectra were collected at 0° tilt angle between the sample surface normal and the direction of the analyzer (normal emission). Measured data (■), fits, and fitting components are included. For detailed assignments, see text.

as will be discussed later. The small peak around 533.5−533.8 eV is probably due to adsorbed water.

The Fe 2p region in the spectrum of the iron substrate contains signals both from metallic iron and from oxidized species, indicating that—similarly to the copper substrate—the surface oxide layer is again not thicker than a few nanometers. A metallic Fe $2p_{3/2}$ peak was found at 707.0 eV, while the broad band of oxidized iron was centered around 710.8−711.0 eV, which is characteristic of Fe^{3+} ions.[73] The main peak of the O 1s region (see Figure 1) lies at 530.1−530.3 eV, which is due to oxygen bound to Fe ions. Although the large peak width of the iron oxide related feature of the Fe 2p spectrum prevents the detailed analysis of the Fe^{3+}-containing species, we believe that the surface layer contains a significant amount of hydroxyl groups, as suggested by the strong O 1s component at 531.6−531.9 eV.

The C 1s signals can be attributed to the hydrocarbon contamination, which develops within minutes on most surfaces exposed to air. The main component found at 285.0 eV is due to aliphatic carbon atoms, a strong peak at 288.6 eV can be assigned to carbon atoms in −C=O bonds, while a weaker component at 286.5−286.7 eV arises from carbon atoms in C−O groups.

Structural Characterization of the LB Films: Quantitative XPS Analysis. Survey scans of the C18P and C18N LB films deposited on copper and iron substrates revealed that the major constituents of the surface layers are carbon and oxygen. The substrate-related metal lines are well observable, indicating that the thickness of the LB overlayer is still not larger than a few nanometers. Phosphorus and nitrogen signals from the headgroups are also detectable, showing that the film preparation was successful, while peaks from other chemical elements are not identifiable.

In the following, first an estimation of the LB layer thickness and orientation will be given, using the quantitative evaluation

Solid Surfaces Modified by Monolayers

J. Phys. Chem. B, Vol. 110, No. 17, 2006 **8705**

of the intensities of the LB film and substrate-related peaks. We will then, in the next section, analyze the chemical state information obtained from the binding energies of the C 1s and the P 2p or N 1s lines, to get some insight into the bonding mechanism of the C18P and C18N molecules to the substrates.

As was mentioned above, the untreated substrates are covered by a thin hydrocarbon contamination and metal oxide layer. Detailed analysis confirms that the contamination is still present after deposition of the LB films (see below). Therefore, the substrate will be described as a semi-infinite metal covered by a few nanometer thick layer containing metal oxide and hydrocarbons. It should be noted that although there are indications in the literature that the contamination may be incorporated into the metal oxide film,[76] the assumption that the hydrocarbon−metal oxide overlayer is regarded as a single layer is still an approximation used primarily for reducing the number of the free parameters of the model. The composition of this metal oxide−hydrocarbon mixed layer is deduced from the analysis of the untreated substrate. A necessary parameter for the calculations is the density of the individual layers. As a consequence of the assumed incorporation of hydrocarbons, the density of the hydrocarbon−metal oxide film was estimated to be somewhat smaller than the bulk density of the corresponding metal oxide: in the case of iron 3.5 g/cm^3 was chosen, whereas for copper 5.0 g/cm^3 was chosen. It is worth mentioning that the exact value does not strongly influence the results obtained for the parameters of the LB layers.

As far as the LB films are concerned, two types of models were tested. In one of them the tails and the headgroups were considered as separate layers. The composition of these regions was determined from the formulas of the hydroxamic and phosphonic acids. The density of the tail region was, according to the bulk density of long chain aliphatic hydrocarbons, chosen to be 0.8 g/cm^3. The choice is confirmed by the fact that the value is in excellent agreement with the density derived using the published pressure−area isotherm of octadecylphosphonic acid.[77] The density of the headgroup layer was estimated using geometrical parameters of the headgroup, and approximate values of 1 g/cm^3 for the hydroxamic acid and 1.8 g/cm^3 for the phosphonic acid were used. In the second LB film model, a disordered layer with homogeneous depth distribution of the headgroups was assumed. The layer density in this model was 0.8 g/cm^3 for both kinds of headgroups.

It is important to note that—due to the presence of the contamination—a given peak such as the aliphatic component of the C 1s band may contain contributions from several layers. Thus, at a fixed detection angle numerous combinations of oxide−hydrocarbon layer composition and LB layer thickness can reproduce the same relative intensities. As a result, the use of the angle-dependent XPS analysis is absolutely necessary for reliable structural information. In the case of iron-supported LB layers, extensive angle-dependent measurements were allowed by the relatively small radiation damage. On the contrary, in the case of the copper substrate only data measured at 0° and 55° were used for the quantitative analysis. In all cases at least two independently prepared samples were characterized to check the reproducibility of the LB film deposition.

LB Films on Iron Substrate. Analysis of several empty iron substrates indicated that the thickness of the hydrocarbon−metal oxide film is typically 3.3−3.5 nm. Neither this value nor the composition of the layer had to be significantly adjusted when fitting the angle-dependent data obtained for the LB film covered substrates, indicating that the LB film molecules do not displace the contamination. Only the amount of oxygen in hydroxyl
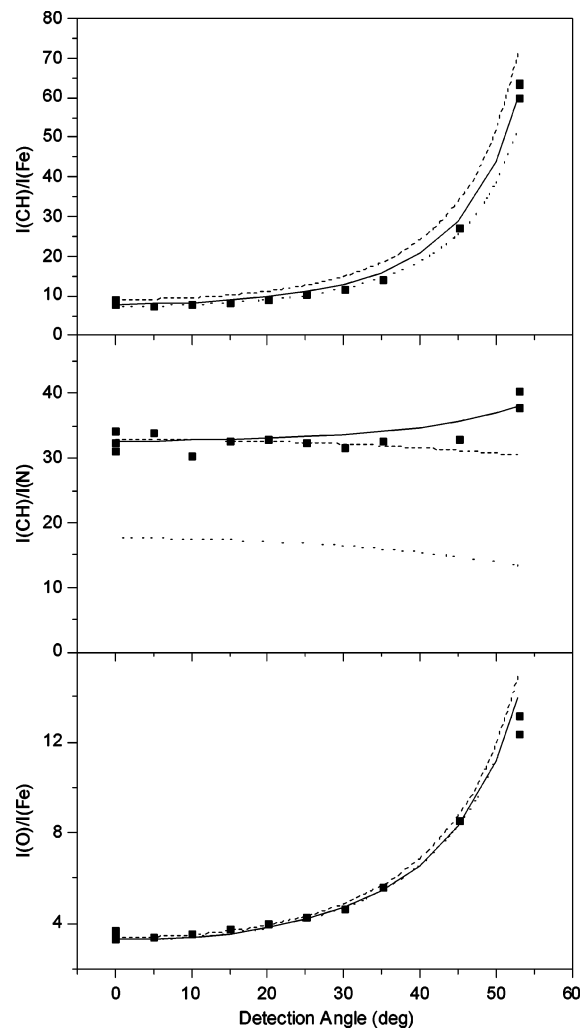

Figure 2. Intensity ratios of selected characteristic photoelectron lines of the C18N film on iron substrate. I(CH) corresponds to the aliphatic component of the C 1s signal, I(N) is the total nitrogen intensity, I(Fe) means the Fe 2p intensity attributed to metallic iron, while I(O) stands for the oxygen intensity arising from the iron oxide. Squares (-■-) represent the measured data, (—) is the calculated ratio with the assumption of headgroups pointing toward the substrate, (- - -) was calculated with the assumption of hydrocarbon tails pointing toward the substrate, (· · ·) is the calculated ratio with the assumption of homogeneous distribution of the headgroups.

groups of the hydrocarbon−oxide layer required strong changes during the fitting procedure, namely, a decrease by some 50% was necessary in the presence of both the C18P and C18N LB layer, suggesting that the surface −OH groups of the substrate are involved in the bonding of the LB films (see below).

In Figure 2 typical results of the angle-dependent XPS analysis of a C18N layer on iron substrate are summarized. The graphs show intensity ratios (corrected for sensitivity factors including cross sections, analyzer transmission and angular distribution) of characteristic peaks of the film and/or the substrate as the function of the detection angle of the photoelectrons with respect to the sample surface normal. Multiple data points at certain angles correspond to several measurements on the same sample.

Lines were generated by calculating the expected intensity ratios of different hypothetical model structures. The best overall fit was obtained with the model assuming an ordered hydroxamic acid monolayer with its headgroup toward the substrate. The thickness of the layer containing the tails turned out to be in this particular case 1.9 nm, while the headgroup layer was

TABLE 1: Estimated Structural Parameters (nm) of the Empty Iron Substrates and the C18P and C18N LB Films on Iron

	sample		
layer	empty substrate	C18P/iron	C18N/iron
hydrocarbon tail		1.9–2.1	1.9–2.1
headgroup		0.27–0.31	0.33–0.38
iron oxide and contamination	3.3–3.5	3.4–3.5	3.3–3.5

TABLE 2: Estimated Structural Parameters (nm) of the Empty Copper Substrates and the C18P and C18N LB Films on Copper

	sample		
layer	empty substrate	C18/copper	C18N/copper
hydrocarbon tail		2.0–2.2	2.0–2.1
headgroup		0.3–0.35	0.3–0.34
copper oxide and contamination	3.5–4.0	3.9–4.0	3.5–3.7

0.35 nm. Although the model assuming an ordered monolayer with tails toward the substrate reproduces quite well the $I(CH)/I(Fe)$ or the $I(O)/I(Fe)$ ratio, the calculated nitrogen signal is much stronger than the measured data (the calculated $I(CH)/I(N)$ ratio is too small). The third model assuming a disordered structure with a random depth distribution of the headgroups gives a somewhat better agreement between the measured and the calculated ratios, although the discrepancies at larger tilt angles are again evident.

Very similar results were obtained in case of the C18P samples. Typical thickness values of LB films on iron are summarized in Table 1. The sample-to-sample scatter is small, indicating the good reproducibility of the film preparation process. The expected error of the data for the LB layers due to the uncertainity of the parameters used in the calculations (especially density) is on the same order as the sample-to-sample scatter, while for the oxide layers deviations may be more significant (up to 25–30%).

LB Films on Copper Substrates. A similar analysis was carried out on the LB films supported on copper. The parameters of the 3.5–4 nm thick hydrocarbon–copper oxide layer are—similarly to the behavior of the iron supported samples—generally not influenced by the LB layer deposition, apart from the concentration of the surface hydroxyls, where again a strong decrease was necessary. Although a complete angle-resolved XPS measurement was impossible in this case, for reproducing the intensity ratios obtained at 0° and 55° detection angles again the model assuming ordered hydroxamic or phosphonic acid monolayer with headgroups toward the substrate turned out to be the best. The typical thickness values of the C18P and C18N layers on copper are summarized in Table 2. As far as the uncertainities are concerned, the same comment applies as in the case of the iron substrates.

In summary, quantitative evaluation of the XPS intensity data in all investigated cases indicates that the LB film deposition process results in formation of well-reproducible coatings consisting of a single hydroxamic acid or phosphonic acid layer. The molecules are connected to the substrate via their headgroups. The structure of the C18P and C18N films seem to be very similar, independently from the substrate: the thickness of the layer of the hydrocarbon tails is typically 1.9–2.1 nm, while the layer of headgroups is about 0.3–0.35 nm thick. Since according to our density functional theory calculations the total length of the C18P and C18N molecules is around 2.5 nm, the

tilt angle of the carbon chains may be 20–30° with respect to the sample surface normal.

Bonding of the LB Films: Qualitative XPS Analysis. The observation that the headgroups of the investigated LB films turn to the substrate allows us to discuss the binding energy data in terms of bond formation between the phosphonic acid and hydroxamic acid molecules and the substrate surfaces. In addition, direct comparison between the LB film results obtained here and data reported in the literature for self-assembled monolayers[78–83] becomes possible, as both systems adapt the same bonding configuration.

C 1s Region. Analysis of the C 1s region of both kinds of LB materials on both substrates indicates that the spectra are very similar, but they are significantly different from the spectrum of the contamination. The main contribution to the C 1s signal comes from a component at 284.8–285.0 eV binding energy which arises from the carbon atoms in C–C, C–H bonds of the aliphatic tails. The component at 286.5–286.7 eV is usually attributed to carbon atoms in C–O bonds,[73] but both carbon atoms in the C–P bond[81,82] and the carbonyl moiety of the hydroxamic acid headgroup adsorbed on metal surfaces[78] are expected to give a contribution to this binding energy region. The third component at 288.3–288.5 eV, which is particularly strong in the spectrum of the empty substrate, is due to carbonyl groups.[73] According to literature data, no carbon signal is expected from the LB layers at this binding energy.

Thus, although the C 1s spectra prove that the substrates became modified by the LB layer, the data also give evidence that the contamination is still present and has to be taken into account when interpreting the XPS results. The same restriction is valid for the O 1s data. As there are no reliable ways to distinguish between C 1s signals from the headgroups and the C–O groups in the contamination, or O 1s signals from the surface hydroxyls, –OH groups of the headgroups, and the contamination, a significant part of information on the bonding of the C18P and C18N molecules is lost. Nevertheless, the P 2p and N 1s lines can still provide important data about the chemical processes between the molecules of the LB layer and the substrate.

P 2p and N 1s Core Levels. In Figure 3 P 2p and N 1s lines from the headgroups of C18P and C18N layers are presented.

The doublet nature of the P 2p peak was taken into account during fitting: the spectrum was fitted with components consisting of two lines with identical width, 2:1 intensity ratio, and 0.8 eV separation.[73] The fitting components shown in Figure 3 are the unresolved doublets. The spectra taken on iron substrate can be well described by one component with a P $2p_{3/2}$ peak at 132.6–133.0 eV, while fitting of the spectra measured on copper always required a second component with P $2p_{3/2}$ binding energy at 134.0–134.3 eV. According to the data in the NIST database,[73] this minor component can be assigned to a fully protonated phosphonic acid headgroup. The main component shifted toward lower binding energies indicates the presence of deprotonated headgroups such as $-PO_3^{2-}$ or $-HPO_3^{-}$,[73,80] indicating the chemical interaction between the LB film molecules and the substrates. It is worth noting that the P $2p_{3/2}$ peak of phosphonic acid molecules adsorbed on transition metal surfaces is found typically at 133 eV binding energy,[79,82,83] indicating that deprotonation is a common sign of bonding of the headgroups to the substrate. The differences in the extent of deprotonation suggest somewhat different bonding properties on iron and copper.

The N 1s spectra indicate again that the interaction between the hydroxamic acid headgroup and iron or copper can be
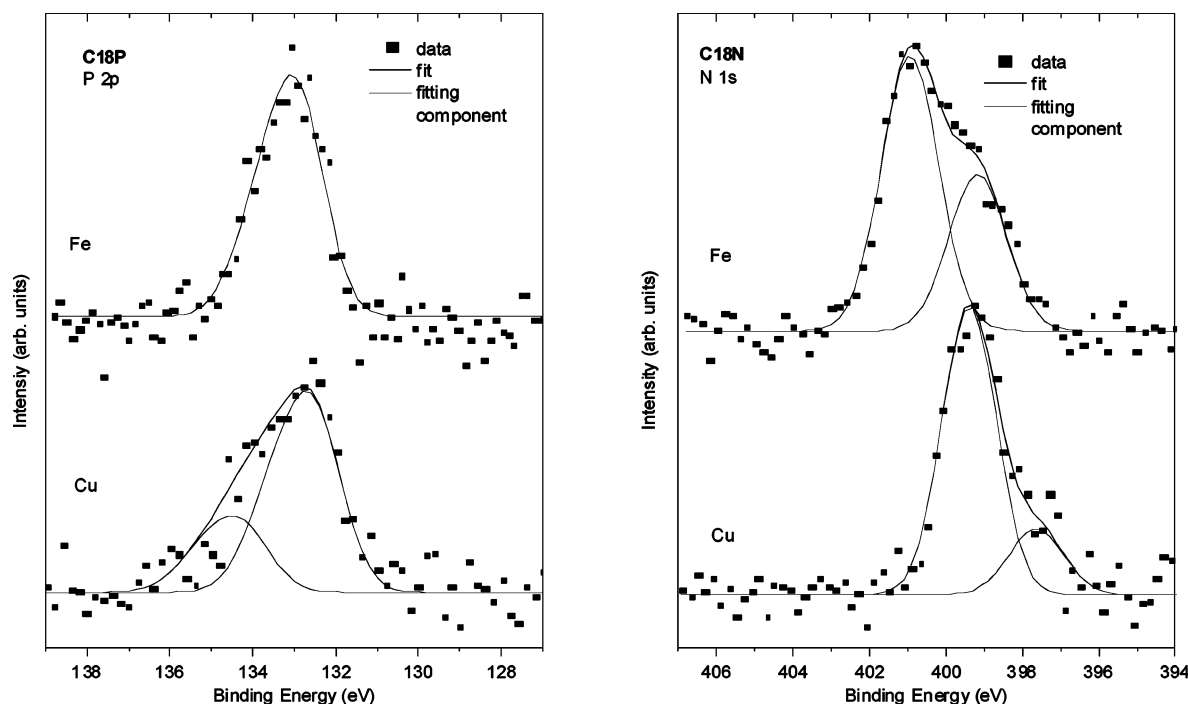
Figure 3. P 2p region of C18P (left) and N 1s region of C18N (right) LB films on copper and iron substrate. Measured data (■), fits, and fitting components are included. Spectra were measured at 0° tilt angle. For detailed assignments, see text.

different. On iron the main component lies at 400.9 eV binding energy, which can be attributed to protonated hydroxamic acid.[78] The slightly smaller peak at lower binding energy (399.1−399.2 eV) is due to the deprotonated headgroups. On the other hand, the main peak on copper can be found at a binding energy characteristic of deprotonated hydroxamic acid (399.2−399.4 eV), which suggests a much stronger deprotonation when compared to iron. A similarly high level of deprotonation was observed in the case of self-assembled monolayers of hydroxamic acids on copper.[78] The small peak at 397.5 eV may even indicate the formation of direct Cu−N bonds as proposed in the case of adsorption of aminopyrimidine on oxidized Cu.[84]

Cu 2p Core Levels. A minor but important change induced by the LB film deposition was observed in the structure of the Cu 2p substrate lines, which completes the information about the bonding mechanism of the LB film molecules.

In Figure 4 the Cu $2p_{3/2}$ peak of an empty substrate can be compared with the data obtained on samples with C18N and C18P LB films. The Cu $2p_{3/2}$ spectrum of an ion bombardment cleaned and contamination- and oxide-free sample serves as reference. The intensities are scaled together for the sake of better visibility. The main peak at 932.6−932.8 eV contains contributions both from metallic copper and Cu^{+} ions of Cu_2O, as described above, while the shoulder at around 935.0−935.3 eV found in all but the ion bombarded sample can be assigned to Cu^{2+} ions in a thin $Cu(OH)_2$ layer.[73,74] The satellite characteristic for Cu^{2+} ions is also clearly observable around 941−943 eV (not shown).

Inspection and fitting of the spectra reveal that deposition of the LB layers results in a significant decrease of the hydroxide-related signal. This observation, along with the results indicating the deprotonation of the hydroxamic acid and phosphonic acid headgroups, strongly suggests that both types of molecules bond to the substrate via a reaction involving the hydroxyl groups of the substrate surface. The most probable reaction is the condensation of the −OH groups in the headgroups and the surface hydroxyl groups, accompanied by elimination of water molecules. This kind of bonding reaction was proposed for self-
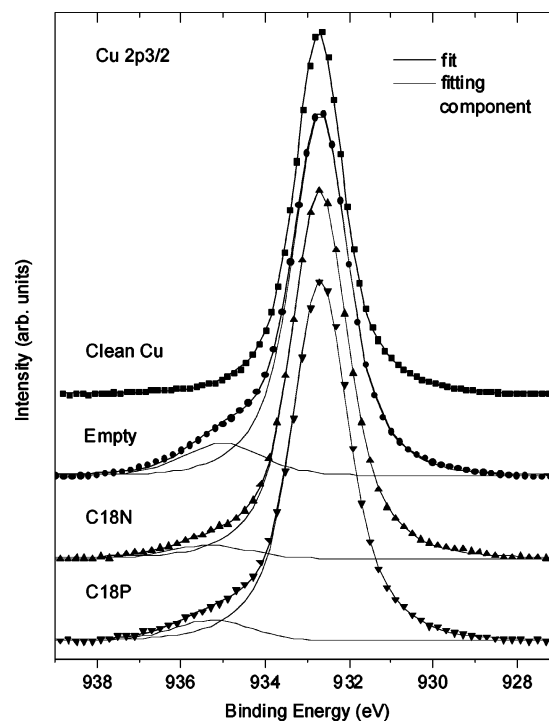

Figure 4. Cu $2p_{3/2}$ peak of an ion bombardment cleaned reference sample (■), an empty copper substrate (●), a C18N/copper (▲), and a C18P/copper (▼) sample. Spectra were recorded at 0° tilt angle. Note the decrease of the shoulder due to Cu^{2+} ions upon LB film deposition.

assembled monolayers of phosphonic acids on zirconium oxide[85] or phosphoric acids on tantalum oxide.[80] In addition, the bond formation between the copper substrate and the C18N or C18P molecules seems to decrease the Cu^{2+} character of the ions in the surface oxide layer.

As was mentioned above, the complex structure of the Fe 2p spectrum renders separation of the surface hydroxyl-related signals very difficult. According to the observed deprotonation, however, we believe that the bonding mechanism of the C18P
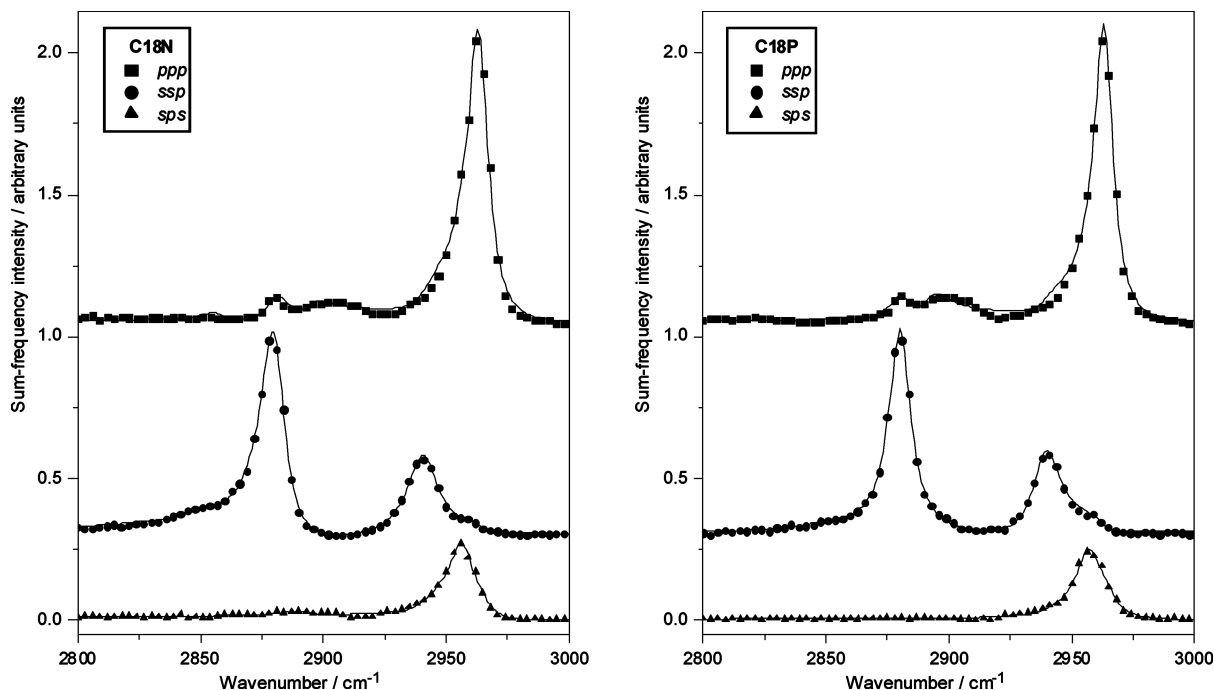
Figure 5. Sum-frequency ppp (rectangles ■), ssp (circles ●), and sps (triangles ▲) spectra of (a) C18N and (b) C18P Langmuir−Blodgett monolayers on glass. Symbols are measured data points; solid lines are fits to eq 3. Spectra belonging to the same species are scaled by a common factor such that the baseline-to-peak height of the ppp spectrum is equal to 1 arbitrary unit. The ppp and ssp spectra are displaced vertically for clarity.

and C18N molecules to iron substrates is basically similar to their bond formation on copper. Nevertheless, some differences in the details of the bonding should be present as indicated by the different extent of deprotonation of the same headgroup on iron or copper. These bonding differences may manifest themselves through substrate-dependent changes in the bond strengths, LB coating durability, and corrosion inhibition properties, although establishing of such correlation is out of the scope of the present work.

Although—because of the overlapping peaks of the contamination, as mentioned above—interpretation of the O 1s signals is difficult, quantitative evaluation of the measured intensities always indicated that the amount of −OH groups of the substrate decreased upon LB film deposition (see above), which is in agreement with the proposed bonding mechanism. Nevertheless, a similar study on a hydrocarbon-contamination-free substrate where the assignment of the O 1s signal is unambiguous,[80] would significantly enhance the understanding of the bonding of the hydroxamic and phosphonic acids to transition metal oxides.

Sum-Frequency Spectroscopy Results

The strength of the sum-frequency signals we obtained from the C18P and C18N samples prepared by the Langmuir−Blodgett technique clearly indicates that the formation of ordered monolayers was successful. The sum-frequency spectra of the C18P and C18N LB monolayers on metal surfaces, which are more relevant model systems from the point of corrosion inhibition, are complicated by the nonresonant signal from the metal surface. The spectra from samples on glass substrates are free from this interference and can thus be used as the starting point for studying these systems.

Langmuir−Blodgett Monolayers on Glass. We first discuss the sum-frequency spectra of C18N and C18P LB monolayers obtained from glass substrates. We collected spectra using the ssp, sps, and ppp polarization combinations. The measured sum-

frequency spectra are plotted in Figure 5. The sum-frequency spectra of the C18N and C18P LB monolayers in the C−H stretch region (2800−3000 cm^{-1}) are rather similar.

The assignment of the major peaks in the spectra is well established in the literature.[86] The ssp spectrum is dominated by the symmetric methyl stretch (r$^+$ mode) at ∼2880 cm^{-1}, and the Fermi resonance of the same mode at ∼2940 cm^{-1} (r$^+_{FR}$). The in-plane (r^-_a) and out-of-plane components (r^-_b) of the antisymmetric methyl stretch[87,88] are the dominant peaks in the ppp and sps spectra at 2965 and 2955 cm^{-1}, respectively. Contributions from the symmetric methylene stretch (d$^+$ mode) at ∼2853 cm^{-1} and the antisymmetric methylene stretch (d$^-$ mode) at 2890−2900 cm^{-1} are also observed in the ssp and ppp spectra.

We have fitted the spectra to eq 3 using the six peaks discussed above and give the parameters obtained from these fits in Table 3. As the contribution of the nonresonant background is very small, the ppp spectra could also be satisfactorily modeled setting the φ_m phases of the resonant peaks to zero.

It is seen from Table 3 that the amplitudes of the symmetric and antisymmetric methylene stretches are rather small (the $A_{d^+,ssp}/A_{r^+,ssp}$ ratio is 0.11 for C18P and 0.06 for C18N), indicating that the alkyl chains of both samples only contain a small number of gauche defects.[63,69]

The splitting of the antisymmetric methyl stretch mode into the in-plane and out-of-plane components indicates that the presence of the long polymethylene chain reduces the symmetry of the methyl group to C_s. Equations 5 and 6 thus cannot be used to determine the orientation of the methyl groups in the C18N and C18P LB- layers. Therefore in our analysis we used C_s symmetry for the methyl group. In this subgroup of C_{3v} the methyl symmetric stretch mode belongs to the a' irreducible representation, the lower energy out-of-plane component of the antisymmetric stretch to a'', and the higher energy in-plane component to a'. Using the same type of transformation between the molecular and laboratory coordinate systems as described

Solid Surfaces Modified by Monolayers

J. Phys. Chem. B, Vol. 110, No. 17, 2006 **8709**

TABLE 3: Fitting Parameters (ω_m, Γ_m, and A_m) for the Sum-Frequency Spectra of C18P and C18N LB Monolayers on Glass

C18P

	ω_m (cm^{-1})	$A_{m,\text{ssp}}$	$A_{m,\text{ppp}}$	$A_{m,\text{sps}}$	Γ_m (cm^{-1})
CH$_2$(s) d$^+$	2854	0.465	0.988	0.023	9.7
CH$_3$(s) r$^+$	2880	4.235	−1.759	0.036	5.5
CH$_2$ (as) d$^-$	2893	0.118	−1.503	0.161	6.6
Fermi r$^+_{\text{FR}}$	2939	3.105	−0.583	−0.113	6.8
CH$_3$(as oop) r^-_b	2957	0.073	0.107	2.821	6.2
CH$_3$(as ip) r^-_a	2963	−0.460	4.562	0.505	4.7
A_{NR}		−0.071	0.064	0.041	
φ_{NR} (radian)		−1.603	2.346	−3.036	

C18N

	ω_m (cm^{-1})	$A_{m,\text{ssp}}$	$A_{m,\text{ppp}}$	$A_{m,\text{sps}}$	Γ_m (cm^{-1})
CH$_2$(s) d$^+$	2856	0.289	1.111	−0.230	6.5
CH$_3$(s) r$^+$	2880	5.078	−1.903	−0.120	6.0
CH$_2$ (as) d$^-$	2895	−0.031	−0.849	0.281	6.2
Fermi r$^+_{\text{FR}}$	2940	4.397	−0.761	−0.410	8.0
CH$_3$(as oop) r^-_b	2957	0.351	0.239	2.535	6.0
CH$_3$(as ip) r^-_a	2964	−0.172	5.105	0.693	5.3
A_{NR}		−0.083	0.075	0.097	
φ_{NR} (radian)		0.446	2.733	3.021	

by Hirose et al.,[50] we obtain the following expressions for some relevant components of the susceptibility tensor

$$\chi_{yz,a'} = \frac{1}{4}N_s([\langle\cos\theta\rangle + \langle\cos^3\theta\rangle](\alpha_{aac} + \alpha_{bbc}) +$$

$$2[\langle\cos\theta\rangle + \langle\cos^3\theta\rangle](\alpha_{ccc} - \alpha_{aca}))$$

$$\chi_{yz,a'} = \frac{1}{4}N_s(2\langle\cos^3\theta\rangle\alpha_{aca} - [\langle\cos\theta\rangle -$$

$$\langle\cos^3\theta\rangle](\alpha_{aac} + \alpha_{bbc} - 2\alpha_{ccc})) \quad (8)$$

$$\chi_{yyz,a''} = -\frac{1}{2}N_s[\langle\cos\theta\rangle - \langle\cos^3\theta\rangle]\alpha_{bcb}$$

$$\chi_{yzy,a''} = \frac{1}{2}N_s\langle\cos^3\theta\rangle\alpha_{bcb} \quad (9)$$

The elements of the hyperpolarizability tensor were calculated according to eq 7 and they are listed in Table 4 for C18N. The vibrational frequencies and the derivatives of the dipole moment and polarizability, with respect to the normal coordinates, were obtained from density functional theory calculations.

We assume that the distribution function $f(\theta)$ is a Gaussian function with a mean of θ_0 and standard deviation of σ

$$f(\theta) = \frac{1}{\sqrt{2\pi\sigma}}e^{-(\theta-\theta_0)^2/2\sigma^2} \quad (10)$$

The ensemble averages $\langle\cos\theta\rangle$ and $\langle\cos^3\theta\rangle$ are calculated by the method of Simpson and Rowlen[89]

$$\langle\cos\theta\rangle = K\int_0^\pi \cos\theta\, f'(\theta)\sin\theta\, d\theta$$

$$\langle\cos^3\theta\rangle = K\int_0^\pi \cos^3\theta\, f'(\theta)\sin\theta\, d\theta \quad (11)$$

K is a normalization constant

$$K = (\int_0^\pi f'(\theta)\sin\theta\, d\theta)^{-1} \quad (12)$$

and $f'(\theta)$ is the net distribution function given by

$$f'(\theta) = \sum_{n=-5}^{5} f(2\pi n + \theta) + f(2\pi n - \theta) \quad (13)$$

From eq 9 we find the ratio, $\chi_{yzy,a''}/\chi_{yyz,a''}$, as

$$\frac{\chi_{yzy,a''}}{\chi_{yyz,a''}} = \frac{\langle\cos^3\theta\rangle}{\langle\cos^3\theta\rangle - \langle\cos\theta\rangle} \quad (14)$$

which is identical to the $\chi_{yzy,\text{as}}/\chi_{yyz,\text{as}}$ ratio that one obtains from eq 6 for a methyl group of C_{3v} symmetry. The $\chi_{yyz,a'}/\chi_{yyz,a''}$ ratio on the other hand is different from the $\chi_{yyz,s}/\chi_{yyz,\text{as}}$ ratio from eq 5.

Figure 6a shows the calculated $\chi_{yyz,a'}/\chi_{yyz,a''}$ ratio (a' denotes the methyl symmetric stretch, and a'' the out-of-plane component of the antisymmetric stretch) as a function of the mean tilt angle θ_0, each curve in the plot corresponding to a different value of standard deviation, σ. The $\sigma = 0°$ line corresponds to a δ-function distribution. The horizontal lines represent the experimental $A_{\text{ssp},r^+}/A_{\text{ssp},r_b^-}$ ratios for C18P and C18N obtained from the fits to the ssp spectra. In Figure 6b the calculated $\chi_{yzy,a''}/\chi_{yyz,a''}$ ratio is shown. In this figure the experimental $A_{\text{sps},r_b^-}/A_{\text{ssp},r_b^-}$ ratios have been corrected for the different Fresnel coefficients and geometrical factors entering the expressions for the effective susceptibilities of the ssp and sps spectra.

From the graphical approach one can only give upper limits for the mean tilt angle and the standard deviation. From Figure 6a one finds that the CH$_3$ group of C18N is tilted by ≤24°, while that of C18P is tilted by ≤12°. The values one can read from Figure 6b are $\theta_0 \leq 21°$ for C18N and $\theta_0 \leq 10°$ for C18P. Both the $\chi_{yyz,a'}/\chi_{yyz,a''}$ and the $\chi_{yzy,a''}/\chi_{yyz,a''}$ ratios are significantly higher for C18P than for C18N. Thus both ratios consistently predict either that the methyl group in C18P is tilted by a smaller angle than that in C18N, if similar width of the distribution is assumed, or that the distribution in C18P is narrower than in C18N if identical tilt angles are assumed.

Langmuir−Blodgett Monolayers on Metal Substrates. LB monolayers of C18N and C18P prepared on copper and iron substrates were also studied by sum-frequency spectroscopy. According to the metal surface selection rules an s-polarized IR beam cannot excite a dipole moment along the metal surface,[90] therefore we only recorded the sum-frequency spectra with the ppp and ssp polarization combinations. Generally in our spectra the intensity of the ssp signal is about an order of magnitude lower than the ppp signal. In Figure 7 the ppp sum-frequency spectra of C18N and C18P LB monolayers on copper and iron surfaces are shown. The spectra in this figure are plotted after scaling the baseline-to-peak height of each spectrum to 1 arbitrary unit.

One can immediately see that the sum-frequency ppp spectra of the same adsorbate on different metal substrates are very different. Furthermore, while on copper surfaces (just like on glass) no significant differences are seen between the sum-frequency ppp spectra of C18N and C18P, on iron substrates the ppp spectra of the samples with different headgroups are quite different.

The differences in the sum frequency spectra of C18N and C18P LB monolayers on the different substrates are explained in part by the differences in the refractive indices, and thus different Fresnel coefficients of the substrates, and in part by the differences in the nonresonant contributions. Due to the significant interference from the nonresonant contribution of the metal substrates, the spectra contain negative-going as well as derivative-like peaks, and therefore the amount of contribution from the individual vibrational modes can only be accurately

TABLE 4: The Elements of the Hyperpolarizability Tensor for the Methyl Group Vibrational Modes of C18N Obtained from Density Functional Theory Calculations, Given in the Units of 10^{-27} m^4 V^{-1} s^{-1}

	r^+, a'	r_b^-, a''	r_a^-, a'		r^+, a'	r_b^-, a''	r_a^-, a'		r^+, a'	r_b^-, a''	r_a^-, a'
α_{aaa}	0.249	0.0	−2.115	α_{baa}	0.0	0.0	0.0	α_{caa}	0.0	0.0	1.751
α_{aab}	0.0	0.0	0.0	α_{bab}	0.0	0.826	0.0	α_{cab}	0.0	0.0	0.0
α_{aac}	1.905	0.0	0.238	α_{bac}	0.0	0.0	0.0	α_{cac}	−0.273	0.0	−0.197
α_{aba}	0.0	0.0	0.0	α_{bba}	0.246	0.0	0.908	α_{cba}	0.0	0.0	0.0
α_{abb}	0.0	0.826	0.0	α_{bbb}	0.0	0.0	0.0	α_{cbb}	0.0	1.541	0.0
α_{abc}	0.0	0.0	0.0	α_{bbc}	1.884	0.0	−0.102	α_{cbc}	0.0	0.0	0.0
α_{aca}	0.0	0.0	1.751	α_{bca}	0.0	0.0	0.0	α_{cca}	0.232	0.0	−0.469
α_{acb}	0.0	0.0	0.0	α_{bcb}	0.0	1.541	0.0	α_{ccb}	0.0	0.0	0.0
α_{acc}	−0.273	0.0	−0.197	α_{bcc}	0.0	0.0	0.0	α_{ccc}	1.775	0.0	0.0

derived from fitting the spectra to eq 3. Although, as explained above, the spectra shown in Figure 7 are scaled, fitting of the spectra was carried out before scaling. In these fits the values of the vibrational frequencies, ω_m, and the widths of the spectral bands, Γ_m, were fixed to the values obtained for the same adsorbates on glass substrates. The results of the fits are summarized in Table 5. As mentioned in connection with eq 3, in the case of the ppp spectra the resonant signal from the LB monolayer is combined with the nonresonant signal of the substrate with a different phase, φ_m, for each vibrational band.

The dominant peaks in the ppp sum-frequency spectra of both the C18N and the C18P LB monolayers on copper (parts a and c of Figure 7, respectively) correspond to the symmetric methyl stretch (r^+ mode) at 2880 cm^{-1}, the Fermi resonance at 2940 cm^{-1} (r^+_{FR}), and the in-plane (r_a^-) component of the antisymmetric methyl stretch at 2965 cm^{-1}. These two spectra are very similar to each other in appearance, as not only the amplitudes but also the phases of the dominant peaks are rather close to each other for the two adsorbates, and so are the values of the nonresonant amplitude. The same peaks also dominate the ppp sum-frequency spectrum of the C18P monolayer on iron (Figure 7d); however the absolute value of the nonresonant amplitude is much smaller in this case, and the phases of the dominant peaks also differ from those obtained for the spectra of the LB monolayers on copper. In the case of the ppp spectrum of the C18N monolayer on iron (Figure 7b), there is also an additional large contribution from the out-of-plane component of the antisymmetric methyl stretch (r_b^-) at 2965 cm^{-1}. The amplitudes

and phases of the other vibrational modes are also different from those either for the C18P monolayer on iron or for the C18N monolayer on copper, thus making the ppp spectrum of the C18N LB monolayer on iron appear very different from any of the other spectra.

As in the case of the ppp spectra the resonant contribution has a different phase for each vibrational band, the ratios of the amplitudes from the ppp spectra on metal substrates cannot be used to get information about the orientation of the methyl groups. This information one can in principle obtain from the ssp spectra. The ssp sum-frequency spectra of C18N and C18P LB monolayers on copper and iron surfaces are plotted as symbols in Figure 8.

For each adsorbate/substrate pair, the spectra are dominated by the symmetric methyl stretch (r^+ mode) at 2880 cm^{-1} and its Fermi resonance at 2940 cm^{-1} (r_{FR}^+). This was also the case with the ssp spectra of the C18N and C18P monolayers on glass. The sum-frequency ssp spectra of the C18N and C18P LB monolayers on copper (parts a and c of Figure 8) are very similar, as was also the case with the ppp spectra (parts a and c of Figure 7). The spectra on the iron substrates are also in this case rather different from those on copper, but the differences between the ssp spectra of C18N and C18P on iron (parts b and d of Figure 8) are much less striking than they were in the case of the ppp spectra (parts b and d of Figure 7).

The absolute magnitudes of these spectra are much smaller than of those recorded with the ppp polarization combination thus the signal-to-noise ratios are much smaller, especially in
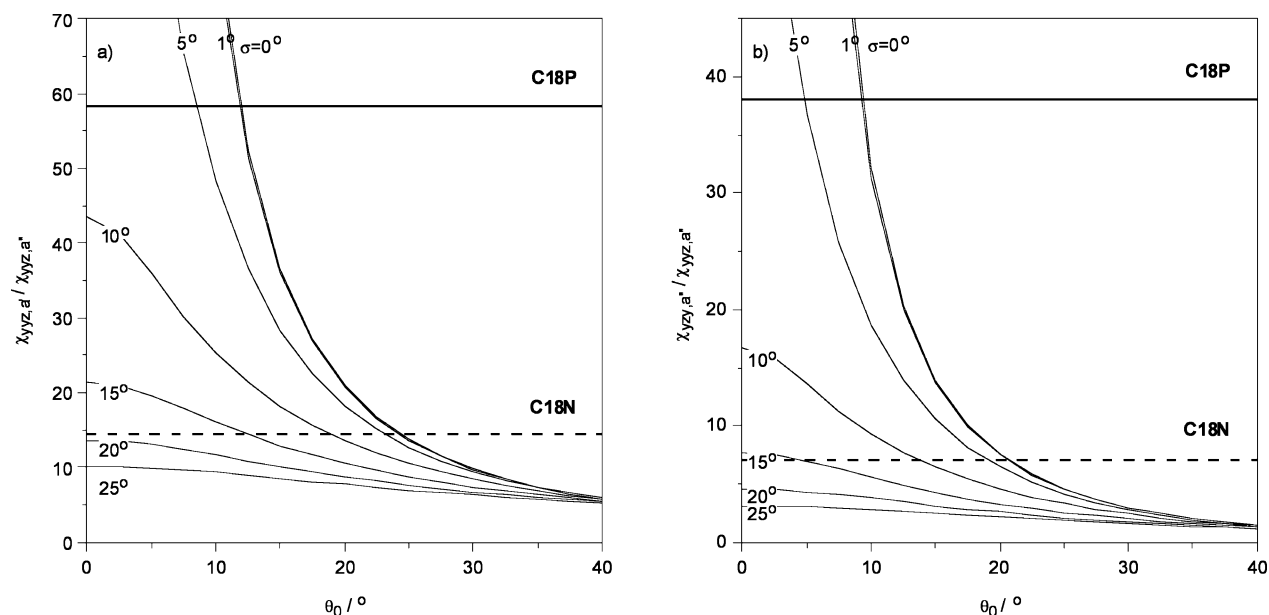

Figure 6. Calculated (a) $\chi_{yyz,a'}/\chi_{yyz,a''}$ and (b) $\chi_{yzy,a'}/\chi_{yyz,a''}$ ratios as a function of the mean tilt angle θ_0. Each curve in the plots corresponds to a different value of standard deviation, σ. The horizontal lines represent the experimental ratios: $A_{ssp,r^+}/A_{ssp,r_b^-}$ in panel (a), and $A_{sps,r_b^-}/A_{ssp,r_b^-}$ (corrected for Fresnel coefficients and geometrical factors) in panel (b).

Solid Surfaces Modified by Monolayers
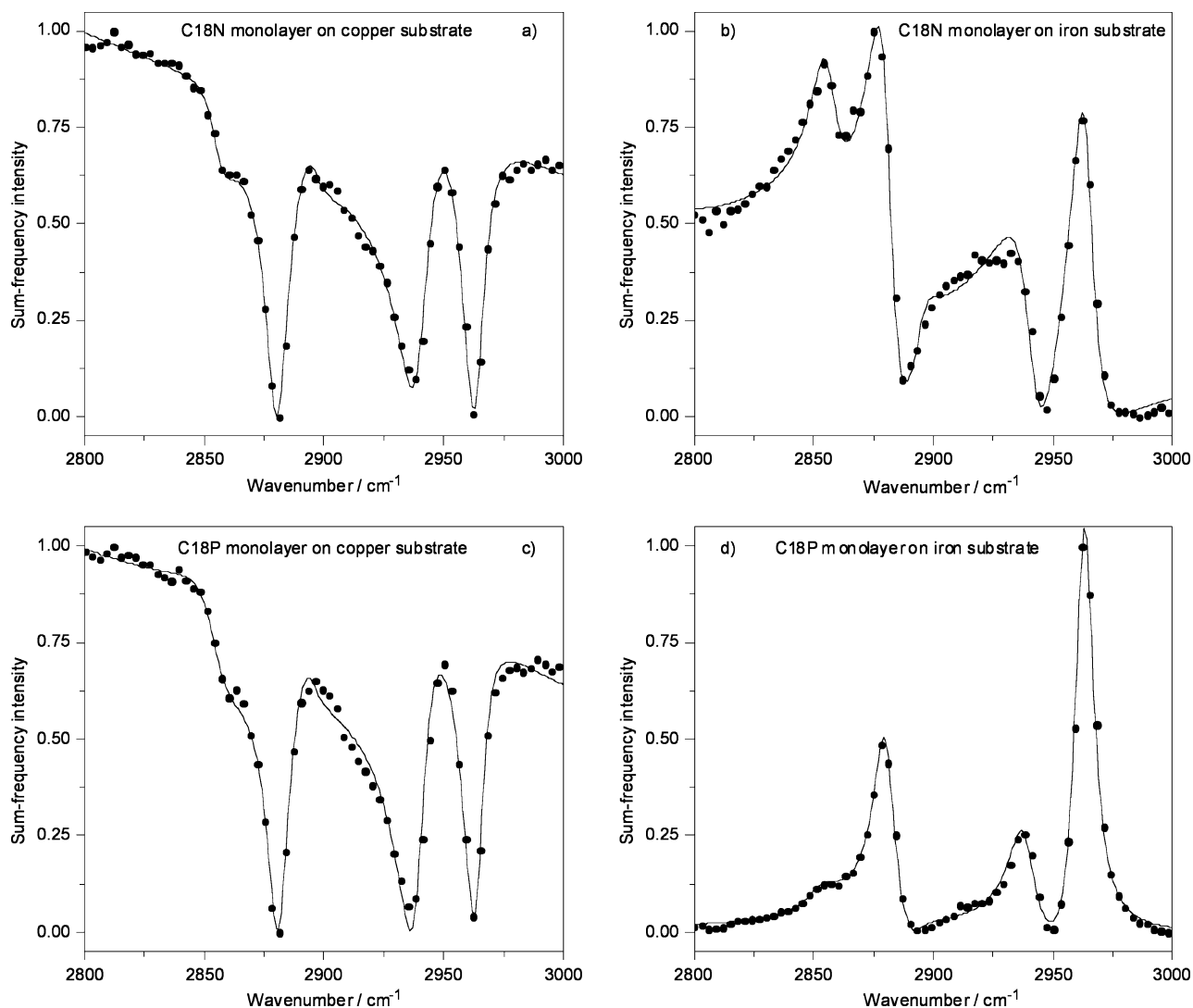
J. Phys. Chem. B, Vol. 110, No. 17, 2006 **8711**

Figure 7. Sum-frequency ppp spectra of Langmuir−Blodgett monolayers of (a) C18N on a copper substrate, (b) C18N on an iron substrate, (c) C18P on a copper substrate, and (d) C18P on an iron substrate. Symbols are measured data points; solid lines are fits to eq 3. See text for the details of the fitting procedure. Spectra are scaled such that the baseline-to-peak height of each spectrum is equal to 1 arbitrary unit.

TABLE 5: Fitting Parameters (A_m and φ_m) for the Sum-Frequency ppp Spectra of C18P and C18N LB Monolayers on Copper and Iron Substrates

| | | | C18N | | | |
| | | | C18N/Cu | | C18N/Fe | |
	ω_m (cm^{-1})	Γ_m (cm^{-1})	$A_{m,ppp}$	φ_m (radian)	$A_{m,ppp}$	φ_m (radian)
CH$_2$(s) d$^+$	2856	6.5	−0.707	2.143	−1.434	3.582
CH$_3$(s) r$^+$	2880	6.0	5.237	−1.69	4.352	−0.476
CH$_2$ (as) d$^-$	2895	6.2	0.550	0.866	0.965	1.658
Fermi r$^+_{FR}$	2940	8.0	5.164	−2.195	6.779	−1.691
CH$_3$(as oop) r^-_b	2957	6.0	−0.835	3.06	−14.084	1.709
CH$_3$(as ip) r^-_a	2964	5.3	3.670	−1.521	−11.556	−2.195
A_{NR}			−4.481		−3.141	

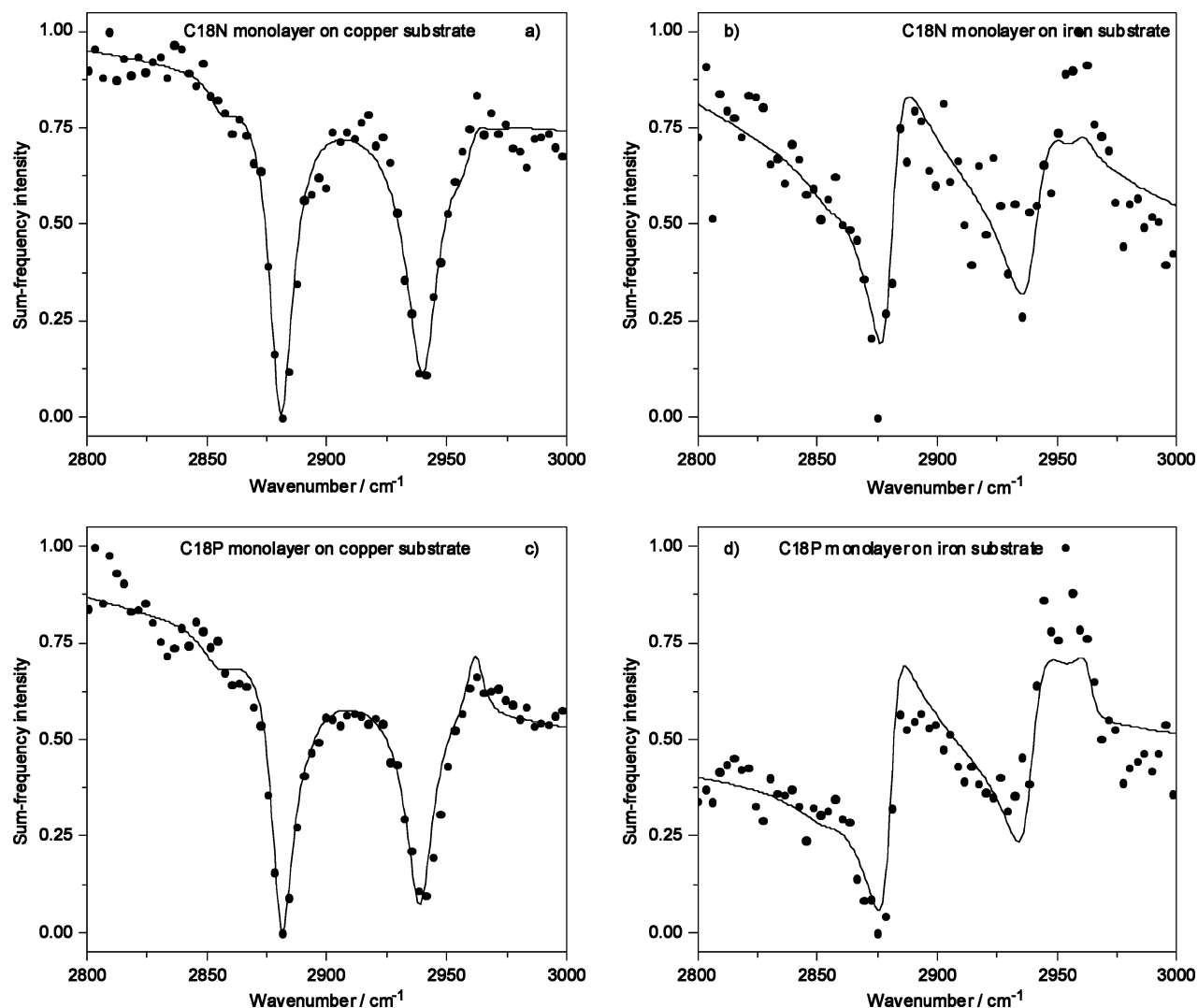| | | | C18P | | | |
| | | | C18P/Cu | | C18P/Fe | |
	ω_m (cm^{-1})	Γ_m (cm^{-1})	$A_{m,ppp}$	φ_m (radian)	$A_{m,ppp}$	φ_m (radian)
CH$_2$(s) d$^+$	2854	9.7	−1.304	2.708	1.124	−1.638
CH$_3$(s) r$^+$	2880	5.5	4.670	−1.763	3.704	−3.021
CH$_2$ (as) d$^-$	2893	6.6	−0.651	−1.948	1.087	−0.440
Fermi r$^+_{FR}$	2939	6.8	6.016	−2.098	3.063	−3.463
CH$_3$(as oop) r^-_b	2957	6.2	−0.806	2.843	1.421	−1.048
CH$_3$(as ip) r^-_a	2963	4.7	2.985	−1.636	4.677	−3.535
A_{NR}			−4.386		0.004	

Figure 8. Sum-frequency ssp spectra of Langmuir−Blodgett monolayers of (a) C18N on a copper substrate, (b) C18N on an iron substrate, (c) C18P on a copper substrate, and (d) C18P on an iron substrate. Symbols are measured data points; solid lines are fits to eq 3. See text for the details of the fitting procedure. Spectra are scaled such that the baseline-to-peak height of each spectrum is equal to 1 arbitrary unit.

the case of the spectra on iron substrates (parts b and d of Figure 8). Therefore from fitting these spectra to eq 3 one could only obtain the resonant amplitudes, and the relevant ratios thereof, presumably with large errors. To nevertheless gain some insight into the orientation of the methyl groups in the LB monolayers of C18N and C18P on the metal substrates, we chose to compare them to the orientation we obtained on glass. We thus fitted the ssp spectra of the monolayers on metal substrates to eq 3 using the vibrational frequencies (ω_m), amplitudes (A_m), and widths (Γ_m) obtained from the fits of the ssp spectra on glass (Table 3). Thus in the fits only the amplitude, A_{NR}, and phase, φ_{NR}, of the nonresonant contribution were varied, together with a single multiplicative factor allowing for the differences in absolute spectral intensities, and an additional factor representing the wavenumber dependence of the nonresonant amplitude. The similarities of the ssp spectra on copper are also reflected in the A_{NR} and φ_{NR} values, for C18N $A_{NR} = 2.504$ and $\varphi_{NR} = -1.580$ and for C18P $A_{NR} = 3.105$ and $\varphi_{NR} = -1.657$. The magnitude and phase of the nonresonant contribution on the iron substrates are quite different from the above values, for C18N $A_{NR} = 7.838$ and $\varphi_{NR} = -0.671$, while in the case of C18P $A_{NR} = 1.251$ and $\varphi_{NR} = -0.595$. The fitted curves are shown in Figure 8 as solid lines. From the figure it can be seen that the ssp spectra measured on metal substrates can be

adequately modeled using the amplitudes obtained from glass, which leads us to the conclusion that by using the Langmuir−Blodgett technique similarly ordered monolayers can be prepared from C18N and C18P on copper and iron surfaces as on glass.

From the detailed analysis of the resonant amplitudes in the sum-frequency spectra of the LB monolayers on glass, and from comparison of these with the ssp spectra measured on metal substrates, we have thus concluded that the alkyl chains of C18N and C18P form an ordered structure on all substrates investigated, with upper limits of the mean tilt angle of the terminal methyl group of ∼20° and ∼10° for C18N and C18P, respectively. From the quantitative evaluation of the XPS intensity data, we found that the tilt angle of the carbon chains is approximately 20−30° with respect to the sample surface normal. Considering that for the C18N and C18P molecules the pseudo-C_3 axis of the methyl group makes an angle of ∼34° with the axis of the hydrocarbon chain, we find that the agreement between the XPS and sum-frequency results is satisfactory.

We have already mentioned that the differences in the appearance of the sum-frequency spectra of the C18N and C18P LB monolayers on the different substrates can be explained by the different nonresonant contributions of the substrates and in the case of the ppp spectra also by the different Fresnel

Solid Surfaces Modified by Monolayers

J. Phys. Chem. B, Vol. 110, No. 17, 2006 **8713**

coefficients. Chemical and physical interactions between the adsorbed monolayers and the atoms and ions in the outermost layers of the substrate surface are likely to influence the optical properties of the latter, thus affecting the appearance of the sum-frequency spectra through the Fresnel coefficients and the nonresonant contributions.

As discussed above, careful inspection of the structure of the Cu 2p$_{3/2}$ substrate lines showed that deposition of the LB layers led to significant decrease of the hydroxide-related component, suggesting that hydroxyl groups of the substrate surface are involved in the bonding of both C18N and C18P molecules to the copper surface. On the other hand, analysis of the P 2p and N 1s lines in the XPS spectra of C18N and C18P LB monolayers indicated a different degree of deprotonation of the headgroups on copper and iron, suggesting somewhat different bonding properties on the two substrates. It is known from the literature that hydroxamic acid molecules can form complexes with various metal ions, including iron and copper ions[91-94] (in certain pH and concentration ranges these complexes have optical absorption in the visible region). Thus one can also assume that molecular interactions similar to those present in the liquid-phase complexes may also exist between hydroxamic acid molecules and surface iron and copper ions. Even though we cannot identify the detailed bonding mechanism and the effect of those to the optical properties of the monolayer-covered substrates, there are apparently ample differences in the interactions between the C18N and C18P molecules in the LB monolayers and the various substrates to account for the differences in the amount of the nonresonant contribution to the sum-frequency spectra.

Conclusions

According to the results of the XPS measurements, the structure of the C18P and C18N films are very similar, independently of the substrate: the thickness of the layer of the hydrocarbon tails is typically 1.9-2.1 nm, while the layer of headgroups is some 0.3-0.35 nm thick. Since the total length of the C18P and C18N molecules is around 2.4-2.5 nm, the tilt angle of the carbon chains may be 20-30° with respect to the sample surface normal and the molecules are connected to the substrate via their headgroups.

XPS spectra of reference samples (substrates without the LB layer) exhibited strong oxygen and significant carbon signals, apart from the metal related peaks, indicating that the initial surfaces are covered by metal oxide as well as a hydrocarbon contamination layer. Nevertheless, the P 2p and N 1s lines can still provide important data about the chemical processes between the molecules of the LB layer and the substrate. The main components of these lines shifted toward lower binding energies indicating the presence of deprotonated headgroups such as $-PO_3^{2-}$ or $-HPO_3^-$. A minor but important change induced by the LB film deposition was observed in the structure of the Cu 2p substrate lines, which completes the information about the bonding mechanism of the LB film molecules. The Cu 2p line includes a component which can be assigned to Cu^{2+} ions in a thin Cu(OH)$_2$ layer. The deposition of LB layers led to significant decrease of the hydroxide-related signal, which indicates that binding of the headgroups to the surface occurs via condensation of the $-OH$ moieties in the headgroups and the surface hydroxyl groups, accompanied by the elimination of water molecules.

The sum-frequency vibrational spectra also confirm that well-ordered monolayers were formed by the Langmuir—Blodgett technique on both metal substrates investigated. Analysis of the resonant peak amplitudes in the sum-frequency spectra of the LB monolayers on glass, used as a model system, yielded upper limits for the mean tilt angle of the terminal methyl groups in the ordered structure of the predominantly all-trans alkyl chains as ~20° for C18N and ~10° for and C18P. As the ssp spectra measured on metal substrates could be satisfactorily modeled using the amplitudes obtained on glass, we concluded that similarly ordered monolayers can be prepared by the Langmuir—Blodgett technique from C18N and C18P on copper and iron surfaces as on glass.

The differences in the appearance of the sum-frequency spectra of the C18N and C18P LB monolayers on the different substrates are due to the different nonresonant contributions of the substrates and to the different Fresnel coefficients. Chemical and physical interactions between the headgroups of the adsorbed monolayers and the atoms and ions in the outermost layers of the substrate surface influence the optical properties of substrate and consequently the Fresnel coefficients and the nonresonant contributions.

References and Notes

(1) Ulman, A. *Chem. Rev.* **1996**, *96*, 1533-1554.

(2) Blodgett, K. A. *J. Am. Chem. Soc.* **1935**, *57*, 1007.

(3) Blodgett, K. A. *Phys. Rev.* **1937**, *51*, 964.

(4) Ulman, A. *An Introduction to Ultrathin Organic Films from Langmuir—Blodgett to Self-Assembly*; Academic Press: London, 1991.

(5) Laibinis, P. E.; Whitesides, G. M. *J. Am. Chem. Soc.* **1992**, *114*, 9022.

(6) Yamamoto, Y.; Nishihara, H.; Aramaki, K. *J. Electrochem. Soc.* **1993**, *140*, 436.

(7) Itoh, M.; Nishihara, H.; Aramaki, K. *J. Electrochem. Soc.* **1994**, *141*, 2018.

(8) Jennings, G. K.; Laibinis, P. E. *Colloid Surf. A* **1996**, *116*, 105.

(9) Nozava, K.; Nishihara, H.; Aramaki, K. *Corros. Sci.* **1997**, *39*, 1625.

(10) Volmer, M.; Stratmann, M.; Viehaus, H. *Surf. Interface Anal.* **1990**, *16*, 278.

(11) Grundmeier, G.; Reinartz, C.; Rohwerder, M.; Stratmann, M. *Electrochim. Acta* **1998**, *43*, 165.

(12) Volmer-Uebig, M.; Reynders, B.; Stratmann, M. *Werkst. Korros.* **1991**, *42*, 19.

(13) Allara, D. L.; Nuzzo, R. G. *Langmuir* **1985**, *1*, 45.

(14) Slotter, N. E.; Porter, M. D.; Bright, T. B.; Allara, D. L. *Chem. Phys. Lett.* **1986**, *132*, 93.

(15) Thoughton, E. B.; Bain, C. D.; Whitesides, G. M. *Langmuir* **1988**, *4*, 365.

(16) Jennings, G. K.; Munro, J. M.; Yong, T. H.; Laibinis, P. E. *Langmuir* **1998**, *14*, 6130.

(17) Xing, L. W.; Shan, Y.; Guo, D.; Lu, T.; Xi, S. *Corrosion* **1995**, *51*, 45.

(18) Aramaki, K.; Shimura, T. *Corros. Sci.* **2004**, *46*, 313.

(19) Wolpers, M.; Stratmann, M.; Viehaus, H.; Streckel, H. *Thin Solid Films* **1992**, *210-211*, 592.

(20) Wolpers, M.; Reynders, B.; Volmer, M.; Stratmann, M. *Proceedings of the 11th International Corrosion Congress on "Innovation and technology transfer for corrosion control"*, Milan, Italy, 1990, Publ. Assoc. Italiano Di Metallurgia, Vol 2., 2.167.

(21) Haneda, R.; Aramaki, K. *J. Electrochem. Soc.* **1997**, *144*, 1215.

(22) Haneda, R.; Aramaki, K. *J. Electrochem. Soc.* **1998**, *145*, 1856.

(23) Lusk, A. T.; Jennings, G. K. *Langmuir* **2001**, *17*, 7830.

(24) Telegdi, J.; Rigó, T.; Kálmán, E. *Corros. Eng. Sci. Technol.* **2004**, *39*, 65-70.

(25) Telegdi, J.; Rigó, T.; Beczner, J.; Kálmán, E. *Surf. Eng.* **2005**, *21*, 107-112.

(26) Telegdi, J.; Rigó, T.; Kálmán, E. *J. Electroanal. Chem.* **2005**, *582*, 191-201.

(27) Rigó, T.; Mikó, A.; Telegdi, J.; Lakatos-Varsányi, M.; Shaban, A.; Kálmán, E. *Electrochem. Solid State* **2005**, *8*, B51-B54.

8714 *J. Phys. Chem. B, Vol. 110, No. 17, 2006*

Keszthelyi et al.

(28) Meucci, S.; Gabrielli, G.; Laibinis, P. E. *Mater. Sci. Eng.*, *C* **1999**, *8−9*, 135−143.

(29) Buselman, J. P.; Valverce, M. B.; de Sánchez, S. R. *Corros. Rev.* **2004**, *22*, 277−305.

(30) Bain, C. D. *J. Chem. Soc.*, *Faraday Trans.* **1995**, *91*, 1281−96.

(31) Miranda, P. B.; Shen, Y. R. *J. Phys. Chem. B* **1999**, *103*, 3292−3307.

(32) Shen, Y. R. *Pure Appl. Chem.* **2001**, *73*, 1589−1598.

(33) Richmond, G. L. *Annu. Rev. Phys. Chem.* **2001**, *52*, 357−389.

(34) Akamatsu, N.; Domen, K.; Hirose, C. *J. Phys. Chem.* **1993**, *97*, 10070−10075.

(35) Ye, S.; Noda, H.; Morita, S.; Uosaki, K.; Osawa, M. *Langmuir* **2003**, 19, 2238−2242.

(36) Holman, J.; Neivandt, D. J.; Davies, P. B. *J. Phys. Chem. B* **2004**, *108*, 1396−1404.

(37) Humbert, C.; Caudano, Y.; Dreesen, L.; Sartenaer, Y.; Mani, A. A.; Silien, C.; Lemaire, J.-J.; Thiry, P. A.; Peremans, A. *Appl. Surf. Sci.* **2004**, *237*, 463−469.

(38) Shon, Y.-S.; Colorado, R.; Williams, C. T.; Bain, C. D.; Lee, T. R. *Langmuir* **2000**, *16*, 541−548.

(39) Berg, O.; David Klenerman, D. *J. Appl. Phys.* **2000**, *90*, 5070.

(40) Song, K. J.; Lagutchev, A. S.; Chuang, T. J.; Huang, J. Y.; Yang, P. K. *Surf. Coat. Technol.* **1997**, *94−95*, 383−389.

(41) Bittner, A. M.; Epple, M.; Kuhnke, K.; Houriet, R.; Heusler, A.; Vogel, H.; Seitsonen, A. P.; Kern, K. *J. Electroanal. Chem.* **2003**, *550*, 113−124.

(42) Nihonyanagi, S.; Ye, S.; Uosaki, K. *Electrochim. Acta* **2001**, *46*, 3057−3061.

(43) Richter, L. J.; Yang, C. S.-C.; Wilson, P. T.; Hacker, C. A.; van Zee, R. D.; Stapleton, J. J.; Allara, D. L.; Yao, Y.; Tour, J. M. *J. Phys. Chem. B* **2004**, *108*, 12547−12559.

(44) Liu, Y.; Wolf, L. K.; Messmer, M. C. *Langmuir* **2001**, *17*, 4329−4335.

(45) Himmelhaus, M.; Eisert, F.; Buck, M.; Grunze, M. *J. Phys. Chem. B* **2000**, *104*, 576−584.

(46) Yeganeh, M. S.; Dougal, S. M.; Polizotti, R. S.; Rabinowitz, P. *Phys. Rev. Lett.* **1995**, *74*, 1811.

(47) Tanaka, Y.; Lin, S.; Aono, M.; Suzuki, T. *Appl. Phys. B* **1999**, *68*, 713−718.

(48) Nishi, N.; Hobara, D.; Yamamoto, M., Kakiuchi, T. *J. Chem. Phys.* **2003**, *118*, 1904−1911.

(49) Follonier, S.; Miller, W. J. W.; Abbott, N. L.; Knoesen, A. *Langmuir* **2003**, *19*, 10501−10509.

(50) Hirose, C.; Akamatsu, N.; Domen, K. *Appl. Spectrosc.* **1992**, *46*, 1051−1072.

(51) *Org. Synth.*; Wiley & Sons: New York, 1971; Collect. Vol. 11, p 67.

(52) Ackerman, B.; Jordan, T. A.; Eddy, C. R.; Sweon, D. *J. Am. Chem. Soc.* **1956**, *78*, 4444.

(53) http://www.ekspla.com/products/SFG/sfg1.htm

(54) Frisch, M. J.; Trucks, G. W.; Schlegel, H. B.; Scuseria, G. E.; Robb, M. A.; Cheeseman, J. R.; Zakrzewski, V. G.; Montgomery, J. A., Jr.; Stratmann, R. E.; Burant, J. C.; Dapprich, S.; Millam, J. M.; Daniels, A. D.; Kudin, K. N.; Strain, M. C.; Farkas, O.; Tomasi, J.; Barone, V.; Cossi, M.; Cammi, R.; Mennucci, B.; Pomelli, C.; Adamo, C.; Clifford, S.; Ochterski, J.; Petersson, G. A.; Ayala, P. Y.; Cui, Q.; Morokuma, K.; Malick, D. K.; Rabuck, A. D.; Raghavachari, K.; Foresman, J. B.; Cioslowski, J.; Ortiz, J. V.; Stefanov, B. B.; Liu, G.; Liashenko, A.; Piskorz, P.; Komaromi, I.; Gomperts, R.; Martin, R. L.; Fox, D. J.; Keith, T.; Al-Laham, M. A.; Peng, C. Y.; Nanayakkara, A.; Gonzalez, C.; Challacombe, M.; Gill, P. M. W.; Johnson, B. G.; Chen, W.; Wong, M. W.; Andres, J. L.; Head-Gordon, M.; Replogle, E. S.; Pople, J. A. *Gaussian 98*, *Revision A.11.4*; Gaussian, Inc.: Pittsburgh, PA, 2002.

(55) Sundius, T. *J. Mol. Struct.* **1990**, *218*, 321.

(56) *PHI Handbook of Photoelectron Spectroscopy*; Moulder, J. F., Stickle, W. F., Sobol, P. E., Bomben, K. D., Chastain, J., Eds.; Perkin-Elmer Corp., Physical Electronics Division: Eden Prairie, MN, 1992.

(57) Mohai, M. *Surf. Interface Anal.* **2004**, *36*, 828. Mohai, M. *XPS MultiQuant*: *Multi-model X-ray Photoelectron Spectroscopy quantification program*, *Version 3.00.16*, 2003; http://www.chemres.hu/aki/XMQpages/XMQhome.htm.

(58) Wagner, C. D.; Davis, L. E.; Zeller, M. V.; Taylor, J. A.; Raymond, R. H.; Gale, L. H. *Surf. Interface Anal.* **1981**, *3*, 211.

(59) Tanuma, S.; Powell, C. J.; Penn, D. R. *Surf. Interface Anal.* **1994**, *21*, 165.

(60) Powell, C. J.; Jablonski, A. *NIST Electron Inelastic-Mean-Free-Path Database−Version 1.1*; National Institute of Standards and Technology: Gaithersburg, MD, 2000.

(61) Shen, Y. R. In *Frontiers in Laser Spectroscopy*, Proceedings of the International School of Physics ''Enrico Fermi'', Course CXX; Hänsch, T., Inguscio, M., Eds.; North-Holland: Amsterdam, 1994; pp 139−165.

(62) Pászti, Z.; Wang, J.; Clarke, M. L.; Chen, Z. *J. Phys. Chem. B* **2004**, *108*, 7779−7787.

(63) Bell, G. R.; Bain, C. D.; Ward, R. N. *J. Chem. Soc.*, *Faraday Trans.* **1996**, *92*, 515−523.

(64) Wang, J.; Pászti, Z.; Even, M. A.; Chen, Z. *J. Am. Chem. Soc.* **2002**, *124*, 7016−7023.

(65) Rangwalla, H.; Schwab, A. D.; Yurdumakan, B.; Yablon, D. G.; Yeganeh, M. S.; Dhinojwala, A. *Langmuir* **2004**, *20*, 8625−8633.

(66) Harp, G. P.; Rangwalla, H.; Yeganeh, M. S.; Dhinojwala, A. *J. Am. Chem. Soc.* **2003**, *125*, 11283−11290.

(67) Ye, S.; Morita, S.; Li, G.; Noda, H.; Tanaka, M.; Uosaki, K.; Osawa, M. *Macromolecules* **2003**, *36*, 5694−5703.

(68) Rao, A.; Rangwalla, H.; Varshney, V.; Dhinojwala, A. *Langmuir* **2004**, *20*, 7183−7188.

(69) Ward, R. N.; Duffy, D. C.; Davies, P. B.; Bain, C. D. *J. Phys. Chem.* **1994**, *98*, 8536−8542.

(70) Oh-e, M.; Lvovsky, A. I.; Wei, X.; Shen, Y. R., *J. Chem. Phys.* **2000**, *113*, 8827−8832.

(71) Lin, S. H.; Villaeys, A. A. *Phys. Rev. A* **1994**, *50*, 5134−5144.

(72) Yeh, Y. L.; Zhang, C.; Held, H.; Mebel, A. M.; Wei, X.; Lin, S. H.; Shen, Y. R. *J. Chem. Phys.* **2001**, *114*, 1837−1843.

(73) Wagner, C. D.; Naumkin, A. V.; Kraut-Vass, A.; Allison, J. W.; Powell, C. J.; Rumble, J. R., Jr. *NIST X-ray Photoelectron Spectroscopy Database*, *Version 3.4*; National Institute of Standards and Technology: Gaithersburg, MD, 2003; http://srdata.nist.gov/xps/.

(74) Barr, T. L. *J. Phys. Chem.* **1978**, *82*, 1801

(75) Cocke, D. L.; Schennach, R.; Hossain, M. A.; Mencer, D. E.; McWhinney, H.; Parga, J. R.; Kesmez, M.; Gomes, J. A. G.; Mollah, M. Y. A. *Vacuum* **2005**, *79*, 71−83.

(76) Allara, D. L.; Nuzzo, R. G. *Langmuir* **1985**, *1*, 45.

(77) Gao, W.; Dickinson, L.; Grozinger, C.; Morin, F. G.; Reven, L. *Langmuir* **1996**, *12*, 6429.

(78) Folkers, J. P.; Gorman, C. B.; Laibinis, P. E.; Buchholz, S.; Whitesides, G. M.; Nuzzo, R. G. *Langmuir* **1995**, *11*, 813.

(79) Gawalt, E.; Lu, G.; Bernasek, S. L.; Schwartz, J. *Langmuir* **1999**, *15*, 8929.

(80) Textor, M.; Ruiz, L.; Hofer, R.; Rossi, A.; Feldman, K.; Hähner, G.; Spencer, N. D. *Langmuir* **2000**, *16*, 3257.

(81) Davies, P. R.; Newton, N. G. *Appl. Surf. Sci.* **2001**, *181*, 296.

(82) Viornery, C.; Chevolot, Y.; Léonard, D.; Aronsson, B.-O.; Péchy, P.; Mathieu, H. J.; Descouts, P.; Grätzel, M. *Langmuir* **2002**, *18*, 2582.

(83) Frateur, I.; Carnot, A.; Zanna, S.; Marcus, P. *Appl. Surf. Sci.* **2006**, *252*, 2757−2769.

(84) Miao, Q.; Yie, X.; Xin, X.; Adachi. H.; Tanaka, I. *Appl. Surf. Sci.* **2001**, *171*, 49.

(85) Gao, W.; Dickinson, L.; Grozinger, C.; Morin, F. G.; Reven, L. *Langmuir* **1996**, *12*, 6429−6435.

(86) MacPhail, R. A.; Strauss, H. L.; Snyder, R. G.; Elliger, C. A. *J. Phys. Chem.* **1984**, *88*, 334.

(87) Bain, C. D.; Davies, P. B.; Hui Ong, T.; Ward, R. N.; Brown, M. A. *Langmuir* **1991**, *7*, 1563−1566.

(88) Guyot-Sionnest, P.; Hunt, J. H.; Shen, Y. R. *Phys. Rev. Lett.* **1987**, *59*, 1597−1600.

(89) Simpson, G. J.; Rowlen, K. L. *J. Am. Chem. Soc.* **1999**, *121*, 2635−2636, Supporting Information.

(90) Somorjai, G. A.; McCrea, K. R. *Adv. Catal.* **2000**, *45*, 385−438.

(91) Farkas, E.; Kozma, E.; Pethõ, M.; Herlihy, K. M.; Micera, G. *Polyhedron* **1998**, *17*, 3331−3342.

(92) Farkas, E.; Enyedy, É. A.; Micera, G.; Garribba, E. *Polyhedron* **2000**, *19*, 1727−1736.

(93) Farkas, E.; Enyedy, É. A.; Zékány, L.; Deák, Gy. *J. Inorg. Biochem.* **2001**, *83*, 107−114.

(94) Farkas, E.; Csóka, H. *J. Inorg. Biochem.* **2002**, *89*, 219−226.